

## Article

# A Multi-Slot Two-Antenna MIMO with High Isolation for Sub-6 GHz 5G/IEEE802.11ac/ax/C-Band/X-Band Wireless and Satellite Applications

Abdullah G. Alharbi <sup>1</sup>, Jayshri Kulkarni <sup>2,\*</sup> , Arpan Desai <sup>3</sup> , Chow-Yen-Desmond Sim <sup>4</sup>  and Ajay Poddar <sup>5</sup> 

- <sup>1</sup> Department of Electrical Engineering, Faculty of Engineering, Jouf University, Sakaka 42421, Saudi Arabia; a.g.alharbi@ieee.org
- <sup>2</sup> Department of Electronics and Telecommunication Engineering, Vishwakarma Institute of Information Technology, Kondhwa, Pune 411048, India
- <sup>3</sup> Department of Electronics and Communication Engineering, CSPIT, Charotar University of Science and Technology (CHARUSAT), Changa 388421, India; arpandesai.ec@charusat.ac.in
- <sup>4</sup> Department of Electrical Engineering, Feng Chia University, Taichung 407, Taiwan; cysim@fcu.edu.tw
- <sup>5</sup> Synergy Microwave Corporation, 201 McLean Boulevard, Paterson, NJ 07504, USA; poddar\_ajay@yahoo.com
- \* Correspondence: jayah2113@gmail.com; Tel.: +91-9552466969

**Abstract:** A tapered symmetrical coplanar waveguide (S-CPW) fed monopole antenna is initially studied. To achieve multiband characteristics, the radiating element of this monopole antenna is loaded with multiple narrow slots and multiple slotted stubs (MSS). The designed slot-loading monopole is further transformed into a two-antenna MIMO type with a gap distance of only  $0.12\lambda$  (at 5 GHz), and thus it has a small overall size of  $32 \times 20 \times 0.8 \text{ mm}^3$ . By deploying five concentric ring elements between the two adjacent antenna elements, the desirable isolation of better than 20 dB is yielded. As the low band and high band operation of the proposed two-antenna MIMO is 81.08% (3.3–7.8 GHz) and 40% (8.0–12.0 GHz), respectively, it can therefore satisfy the Sub-6 GHz 5G New Radio (NR) n77/78/79, IEEE 802.11ac/ax, X-band/C-band wireless and satellite applications. Furthermore, it has shown a desirable gain of above 3 dBi and a radiation efficiency greater than 69% throughout the two bands of interest.

**Keywords:** monopole antenna; two-antenna MIMO; slot loaded; Sub-6 GHz; IEEE 802.11ac/ac; X-band; C-band



**Citation:** Alharbi, A.G.; Kulkarni, J.; Desai, A.; Sim, C.-Y.-D.; Poddar, A. A Multi-Slot Two-Antenna MIMO with High Isolation for Sub-6 GHz 5G/IEEE802.11ac/ax/C-Band/X-Band Wireless and Satellite Applications. *Electronics* **2022**, *11*, 473. <https://doi.org/10.3390/electronics11030473>

Academic Editors: Faisal Tubbal, Ladislau Matekovits and Raad Raad

Received: 15 January 2022  
Accepted: 4 February 2022  
Published: 5 February 2022

**Publisher's Note:** MDPI stays neutral with regard to jurisdictional claims in published maps and institutional affiliations.



**Copyright:** © 2022 by the authors. Licensee MDPI, Basel, Switzerland. This article is an open access article distributed under the terms and conditions of the Creative Commons Attribution (CC BY) license (<https://creativecommons.org/licenses/by/4.0/>).

## 1. Introduction

The main challenging part of designing a compact size MIMO antenna is to obtain a very high isolation of  $>20$  dB between the two adjacent antenna elements without affecting the scattering, radiation, and diversity performances. Therefore, several decoupling techniques have been reported in recent years for compact size planar MIMO antennas with multi-band or broadband operations [1–21]. In [1], a two-antenna MIMO with frequency reconfigurable characteristics is designed using radio frequency micro electro mechanical systems (RF-MEMS) switches. This antenna has a designed footprint of  $32 \times 98 \times 1 \text{ mm}^3$ , and it can switch among the 0.6, 1.8, 2.4, 3.5, and 5.5 GHz bands with isolation  $>15$  dB. However, the use of the RF-MEMS switch makes the antenna design more complex. To reduce the complexity, Ref. [2] has proposed two symmetrically located spider-shaped antennas (of size  $37 \times 56 \times 1.6 \text{ mm}^3$ ) that can operate in the Wi-Fi/WiMAX/Bluetooth and C-band applications. However, it does not cover the entire 5 GHz band. A dual band, a Two-port antenna functioning in a 2.4 GHz and 5 GHz band with a dimension of  $46 \times 20 \times 1.6 \text{ mm}^3$ , is proposed in [3], but the isolation is only around 12 dB. Therefore, a Wang shaped triple-band MIMO antenna with a high isolation of 31 dB is reported in [4], but this antenna has occupied a large area of  $70 \times 52 \text{ mm}^2$ . To achieve smaller dimensions for the MIMO antenna, Ref. [5] has designed a two-antenna MIMO with a planar size of only  $24 \times 20 \text{ mm}^2$ .

Here, a single complementary split-ring resonator (S-CSRR) is loaded into the radiating element to enhance the performance, as well as operating in the X- and Ku-band. In [6], a two-port MIMO monopole antenna with a small size of  $27 \times 16 \times 0.8 \text{ mm}^3$  is reported. This antenna is a single band operation (4.85–7.32 GHz), and it has shown good isolation of  $>15 \text{ dB}$  [6]. To achieve dualband operation with higher isolation, a dualband MIMO antenna (size  $27 \times 21 \times 1.6 \text{ mm}^3$ ) using orthogonal polarisation has been reported [7]. Even though it can yield very high isolation of  $>22.5 \text{ dB}$ , the two operating bands are rather narrow at 4.15% (5.19–5.41 GHz) and 4.81% (7.30–7.66 GHz). To further achieve triple-band operation, a MIMO antenna with a compact size of  $20 \times 14.75 \text{ mm}^2$  has been reported in [8]. The antenna element is composed of an asymmetric coplanar strip (ACS) feedline, along with an inverted L-shaped slot and a meander line to operate in the WLAN (2.4/5.2/5.8 GHz) and WiMAX (2.5/3.5/5.5 GHz) applications. Notably, all the MIMO antennas reported in [1–8] do not apply any decoupling structure between adjacent antenna elements. Hence, they will suffer from low isolation if a wider operating bandwidth is implemented.

The easiest way to reduce the mutual coupling of any two adjacent antenna elements is to apply the spatial diversity method. The advantage of this method is that the MIMO antenna does not require any decoupling structure, such as the one reported in [9] that has a gap distance of 36 mm ( $>1/4$  wavelength) between the two adjacent antennas, and good isolation of  $>30 \text{ dB}$  is achieved. However, applying the spatial diversity method will result in occupying more space and, hence, an increased dimension. To reduce the mutual coupling without occupying much gap distance between the antenna elements, several MIMO antenna designs with different decoupling structures, such as the U-shaped slots [10], T-shape stub [11], comb-shaped structures [12], modified T-shape stub at ground plane [13], and defected ground structures [14–17], have been reported. However, the volume size of [10–17] is between ( $20 \times 35 \times 0.8 \text{ mm}^3$ ,  $560 \text{ mm}^3$ ) and ( $50 \times 50 \times 7 \text{ mm}^3$ ,  $17,500 \text{ mm}^3$ ), and none of these MIMO designs exhibit a very wide operational bandwidth ( $>80\%$ ) and high isolation  $>20 \text{ dB}$  for modern wireless applications with a physical volume size of below or near  $500 \text{ mm}^3$ .

To achieve high isolation without increasing the overall volume of the MIMO antenna, recent decoupling techniques such as the loading of the EBG structure [18,19] and metamaterials [20,21] have been widely used. In [18], the fractal EBG technique is applied to enhance the isolation to 24.67 dB, but the two-antenna MIMO has a volume size of  $38.2 \times 95.94 \times 1.6 \text{ mm}^3$ , and it covers only a narrow single ISM band from 2.39 to 2.48 GHz. Even though the volume size of the antenna in [19] ( $55 \times 28 \times 1.6 \text{ mm}^2$ ) is much less than that of [18], and it has exhibited a wider operating bandwidth of 64.42% (2.01–3.92 GHz), one can see that it has exhibited isolation of only  $>15 \text{ dB}$  after applying the EBG structure. In [20], the textile-based antenna has applied a unique metamaterial inspired decoupling network to enhance the isolation between adjacent antenna elements. The two bands of interest, in this case, are 56% (1.34–3.92 GHz) and 37.4% (4.34–6.34 GHz), and isolation of  $>18 \text{ dB}$  was measured. However, this antenna has a very large dimension of  $100 \times 60 \times 1 \text{ mm}^3$ . To achieve a small volume size of  $47.5 \times 40 \times 1.6 \text{ mm}^3$ , [21] has proposed a single band, two-antenna MIMO monopole that has applied a metamaterial split ring resonator unit to improve the isolation. However, the antenna is a single band operation with a 10-dB impedance bandwidth of 12.3% (3.35–3.78 GHz) and the isolation is only 15 dB.

From the study of literature [1–21], it is observed that the reported MIMO antennas can yield high isolation, but with a narrow operational band or vice-versa. Furthermore, many of them have required a very large volume size. Therefore, in this paper, a compact volume size ( $32 \times 20 \times 0.8 \text{ mm}^3$ ,  $512 \text{ mm}^3$ ) two-antenna monopole MIMO with a dual wideband operation (3.3–7.8 GHz and 8.0–12.0 GHz), as well as high isolation ( $>20 \text{ dB}$ ) for the wireless and satellite applications is proposed. The proposed two-antenna MIMO functions in the Sub-6 GHz 5G NR n77 (3.3–4.2 GHz)/n78 (3.3–3.8 GHz)/n79 (4.4–5.0 GHz), standard C-band uplink (3.7–4.2 GHz)/downlink (5.92–6.425 GHz), extended C-band uplink (3.4–3.7 GHz)/downlink (6.425–6.725 GHz), 802.11ac (5.15–5.85 GHz)/802.11ax

(5.92–7.125 GHz), and X-band radar (8.0–12.0 GHz). Therefore, an integration of the Sub-6 GHz 5G, IEEE 802.11ac/ax, X-band, and C-band into a single antenna along with MIMO configuration would be a good candidate for future wireless and satellite applications. This manuscript is organized as: Sections 2 and 3 explain the geometry and evolution of the monopole element and its characteristics, Section 4 analyses the geometry layout of the two-antenna MIMO along with its working principles. Sections 5 and 6 discuss the results and diversity performances of the proposed two-antenna MIMO. Section 7 compares the proposed two-antenna MIMO with the pioneering state of arts and finally, Section 8 concludes the paper.

## 2. Design Layout of Single Monopole Antenna Element

The design layout and geometry of the single monopole antenna element that will be further applied for realising the proposed two-antenna monopole MIMO are depicted in Figure 1. Here, the radiating section (rectangular radiator) of the monopole antenna is loaded with two narrow L-shaped slots, an inverted-U narrow slot, and two symmetrical MSS (deployed on the right and left side of the rectangular radiator). To achieve better impedance matching, a two-steps co-planar waveguide (CPW) feeding line (of width 1.5 mm and 2 mm) is applied, and the tapered structure that is loaded at the bottom of the rectangular radiator (linked to the feeding line of the CPW) is for yielding a wider operating bandwidth. As seen from Figure 1, the two co-planar ground planes have an area of  $4 \times 7 \text{ mm}^2$  each, and it is slightly truncated, with an air gap of 0.5 mm due to the two-steps CPW feeding line. The antenna structure is engraved on a 0.8 mm FR-4 substrate having a relative permittivity ( $\epsilon_r$ ) of 4.3 and a loss tangent ( $\tan\delta$ ) of 0.025. The overall planar size of this single monopole antenna element is  $20 \times 13 \text{ mm}^2$ .

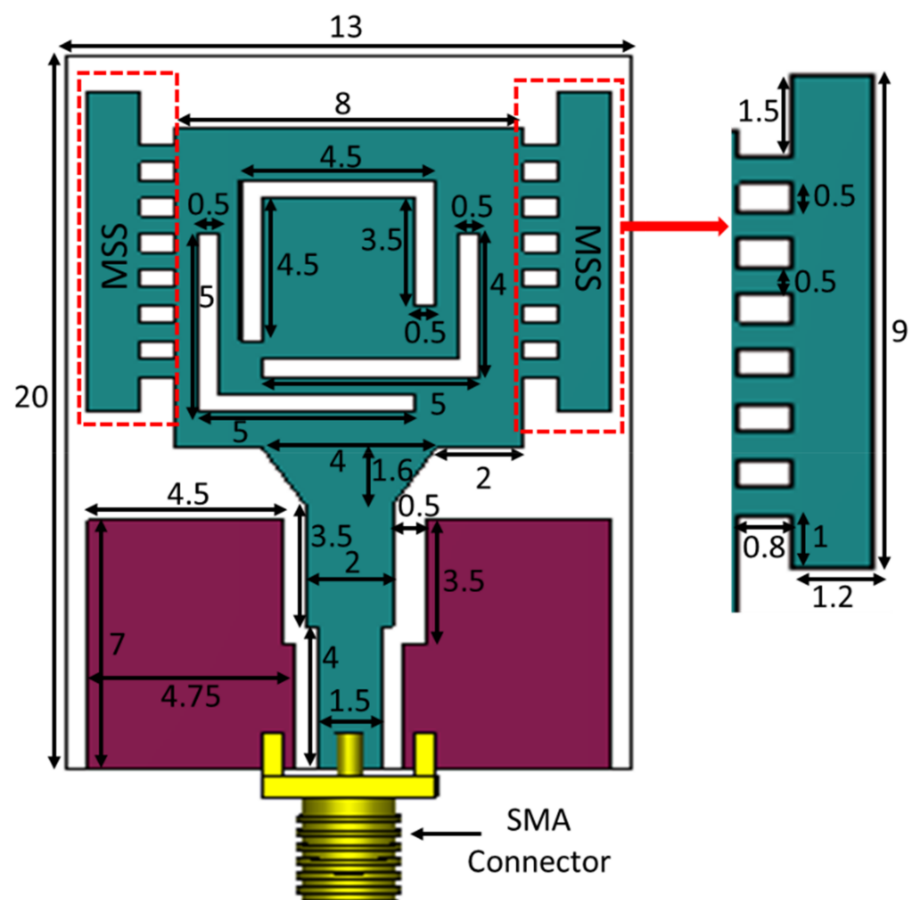


Figure 1. Layout and geometry of single monopole antenna element (all units in mm).

### 3. Antenna Evolution Mechanism

To comprehend the excitation of the two wide operational bandwidths from the single monopole antenna element, this section explains the antenna evolution mechanism including the step-wise design and its associated reflection coefficient curve.

#### 3.1. Step-1: Design of Rectangular Radiator

The antenna design begins with a two-step CPW-fed rectangular radiator with a tapered structure at the bottom, as illustrated in Figure 2a, and it is denoted as ANT#1. Here, ANT#1 was analysed and numerically simulated using the CST Microwave Studio® (CST MWS) software. The width and length of the rectangular radiator is optimised using the CST MWS.

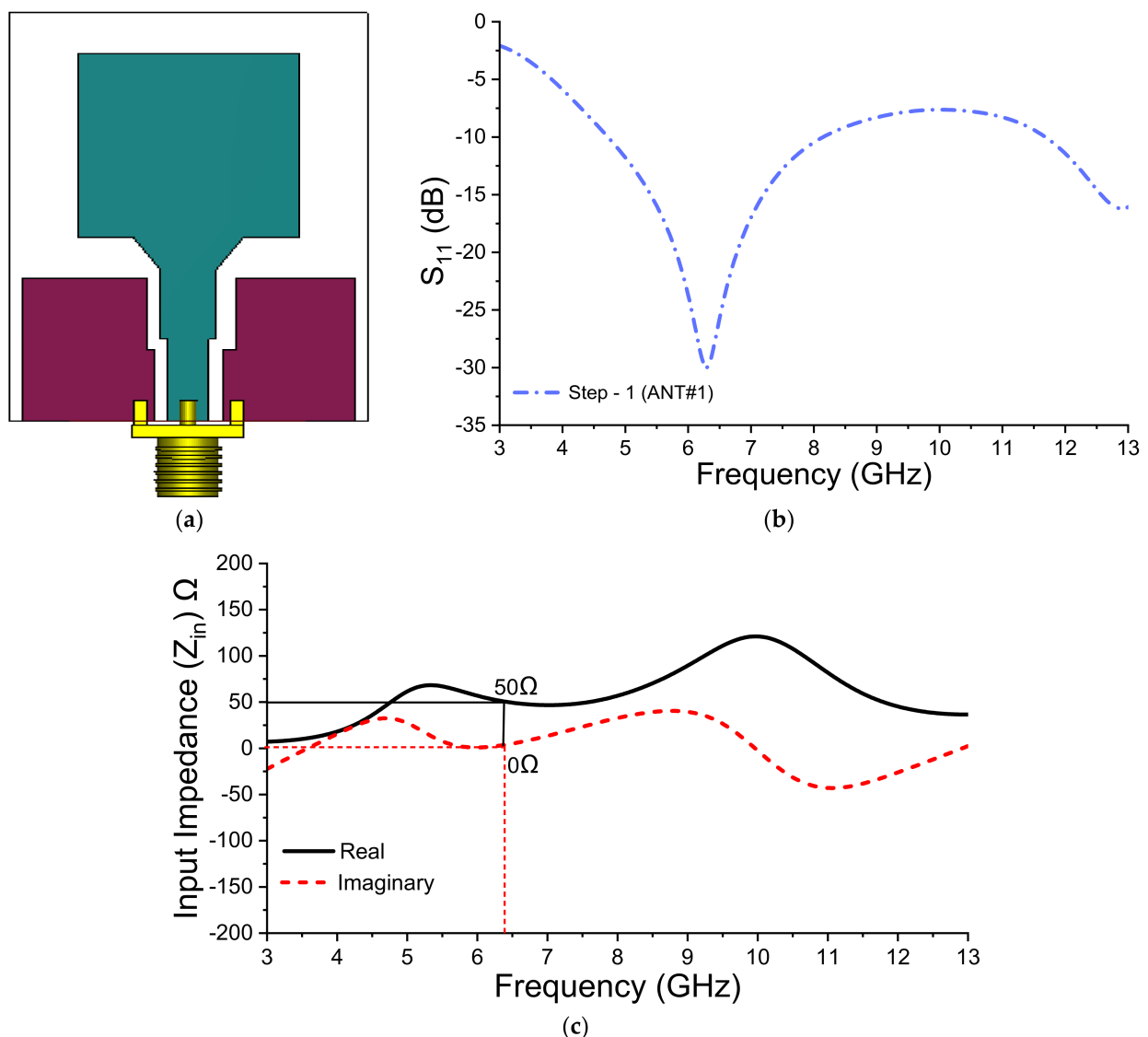


**Figure 2.** Step-1 of single monopole antenna element, (a) ANT#1 structure, (b)  $S_{11}$ , (c) input impedance.

From Figure 2b, it is clearly observed that ANT#1 has successfully induced a wideband operation with a 10-impedance bandwidth of 4.74–8.10 GHz (centred at 6.3 GHz). Thus, it can meet the wideband demand for X- and C-band applications. Figure 2c validates that the incorporation of a rectangular patch, truncated ground planes and a tapered structure offers equal amounts of inductive and capacitive reactance at a resonating frequency of 6.3 GHz. Hence, achieving good impedance matching throughout the operating band (4.74–8.10 GHz).

### 3.2. Step-2: Deployment of MSS on Right and Left Side of ANT#1

As can be seen in Figure 2c, the frequency band generated by ANT#1 is not enough to cover the standard and extended C-band. Therefore, to shift the frequency band towards the lower spectrum and to match the load impedance of  $100\ \Omega$  to the  $50\ \Omega$  feed line, a series open circuit MSS is embedded into the left and right side of the ANT#1 (which forms the ANT#2), without disturbing the feeding arrangement of ANT#1, as shown in Figure 3a. Notably, there are six small slots (each has a size of  $0.8 \times 0.5\ \text{mm}^2$ ) in each MSS (see Figure 1), and these slots are acting as capacitors and behave like an open circuit to block the high inductive reactance across the operating frequency range.

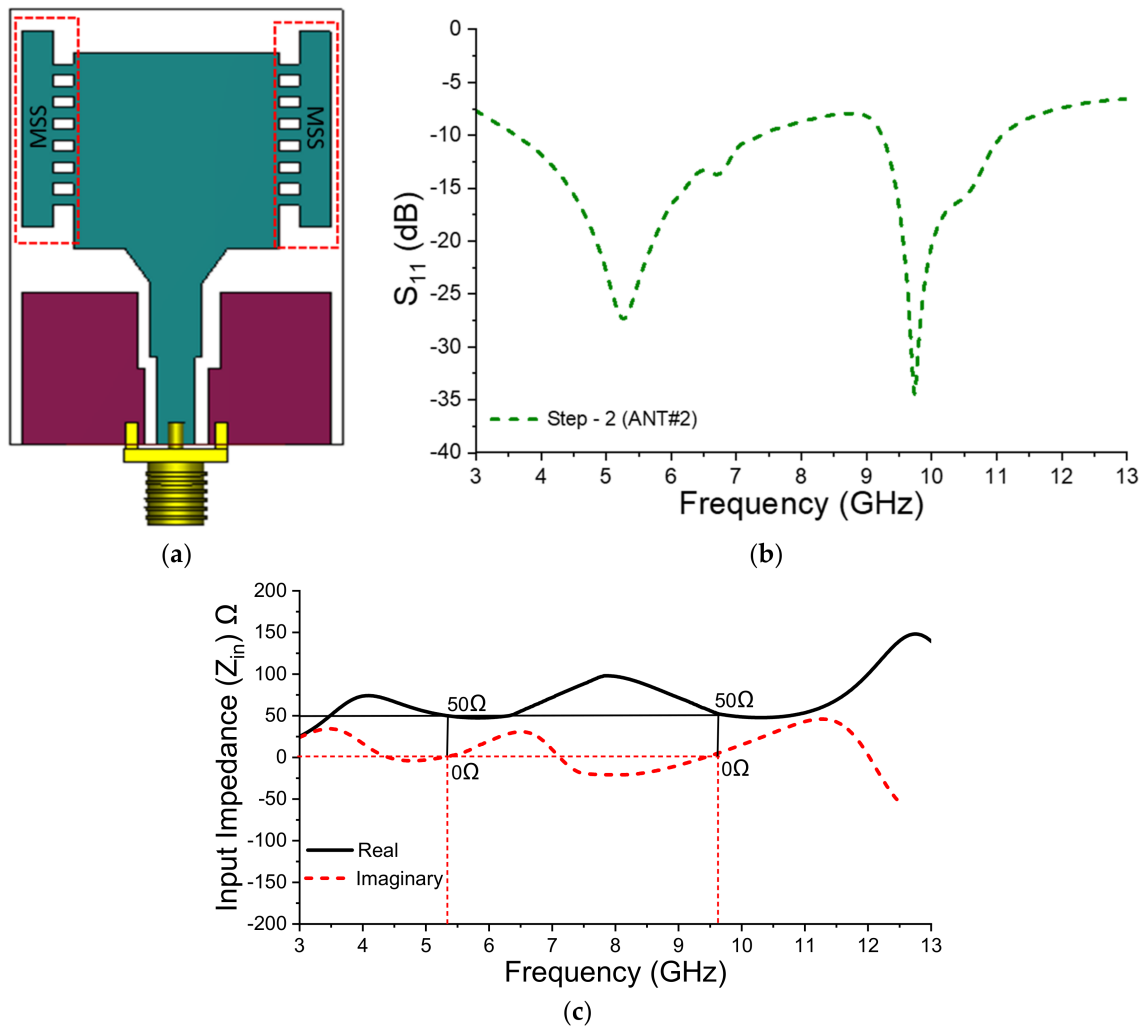


**Figure 3.** Step-2 of single monopole antenna element, (a) ANT#2 structure, (b)  $S_{11}$ , (c) input impedance.

From the reflection coefficient curve of Figure 3b, it is visualised that the incorporation of the two symmetrical MSS into ANT#1 (that forms the ANT#2) can shift the previous frequency mode (6.3 GHz) towards the lower spectrum at approximately 5.3 GHz, and a good 10-dB impedance bandwidth of approximately 3.4–7.0 GHz (low band) is achieved. Meanwhile, ANT#2 can also generate another high band operation with 10-dB impedance bandwidth of 9.4–11.1 GHz. Therefore, ANT#2 is able to operate in the IEEE 802.11ac, C-band and partial X-band applications.

To comprehend the contributions of the MSS that achieves good impedance matching across the two bands of interest, Figure 3c depicts the input impedance  $Z_{in}$  ( $\Omega$ ) diagram of ANT#2. Here, one can clearly see that good impedance matching has been achieved throughout the two operating bands of 3.4–7.0 GHz and 9.4–11.1 GHz, as their resistive

impedances are very much closer to  $50 \Omega$  and their corresponding reactive impedances are near  $0 \Omega$ . This validates that the two symmetrical MSS can aid in achieving good impedance matching across the low band and exciting a new high band.

3.3. Step-3: The Loading of L-Shaped Slots and Inverted U-Shaped Slot

To further integrate the Sub-6 GHz NR 5G bands along with the IEEE 802.11 ac/ax, C-band, and X-band into a single antenna simultaneously, ANT#3 (as shown in Figure 4a) is developed by further loading 3 narrow slots, namely, two L-shaped slots and an inverted U-shaped slot. When these slots are loaded into the rectangular radiator, they get interlocked with each other and aid in reducing the capacitive reactance. Moreover, these slots also help to widen the previous frequency band by forcing the current distribution on the surface of the radiator to flow for a longer time period, as well as diverting the current paths to flow in various directions with various velocities. This results in the merging of all the currents coming from various directions with different velocities and offers a wide bandwidth, which can be seen in Figure 4b that plots the current distributions at 5 GHz for ANT#1 and ANT#3. To illustrate the wideband characteristics of ANT#3, its corresponding reflection coefficient is plotted in Figure 4c. It is clearly seen that ANT# 3 is able to yield a dual bandwidth operation spanning in the range of 81.08% (3.3–7.8 GHz) and 40% (8.0–12.0 GHz) at the resonant frequency of 5.0 GHz and 10.5 GHz, respectively. Figure 4d shows the input impedance diagram of ANT#3. Here, one can see excellent impedance matching throughout the two bands of interest, in which the resistive and reactive impedances are around  $50 \Omega$  and near  $0 \Omega$  across the two bands, respectively. Therefore, ANT#3 is considered for further analysis and will be applied for MIMO applications. The step-wise configuration of ANT#1 to ANT#3 and their associated operating bands are mentioned in Table 1.

Table 1. Step-wise configuration and operating bands of ANT#1 to ANT#3.

Step	Sub-6 GHz 5G NR	IEEE 802.11ac	IEEE 802.11ax	C-Band	X-Band	Impedance Matching
ANT#1	-	Yes	Yes	-	-	Good
ANT#2	-	Yes	-	Yes	-	Good
ANT#3	Yes	Yes	Yes	Yes	Yes	Good

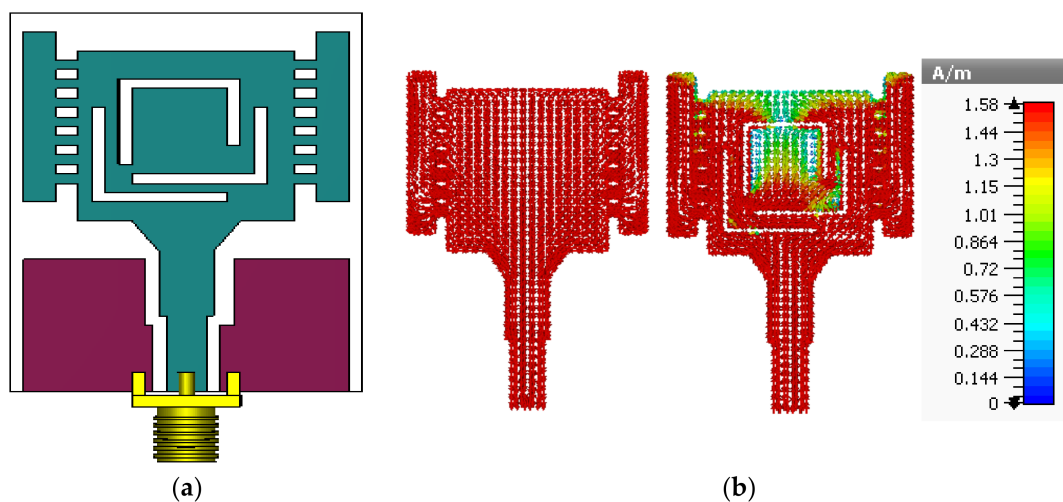
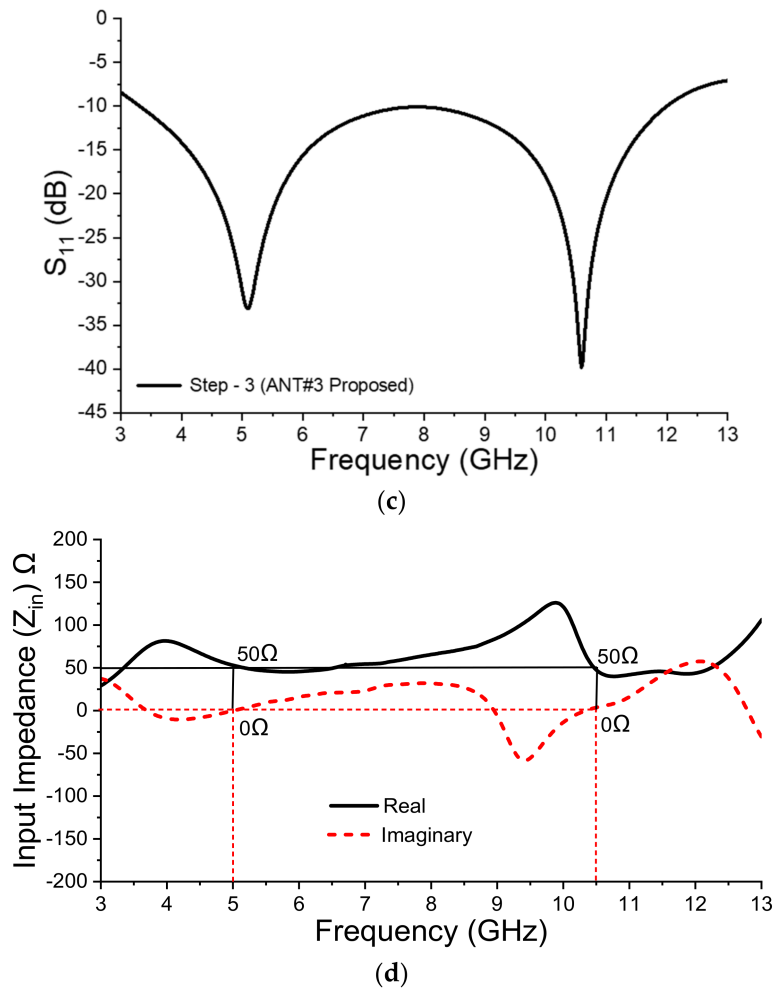


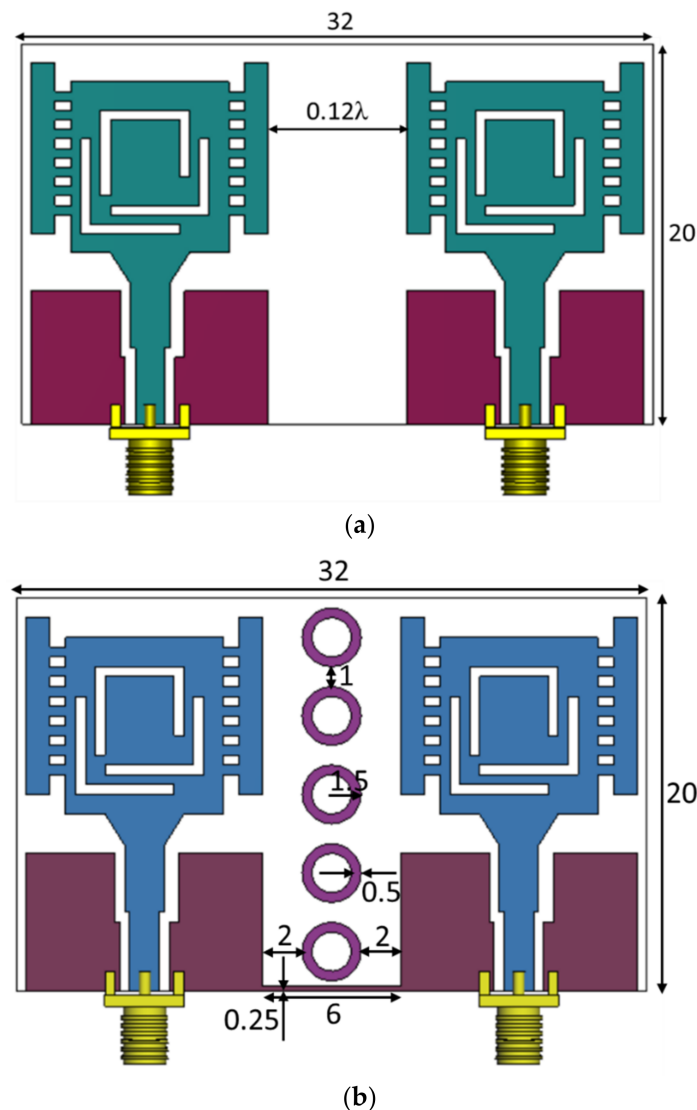
Figure 4. Cont.



**Figure 4.** Step-3 of single monopole antenna element, (a) proposed monopole antenna element, (b) current distributions at 5 GHz, (c)  $S_{11}$ , (d) input impedance.

#### 4. Geometry, Design and Analysis of the Proposed Two-Antenna MIMO

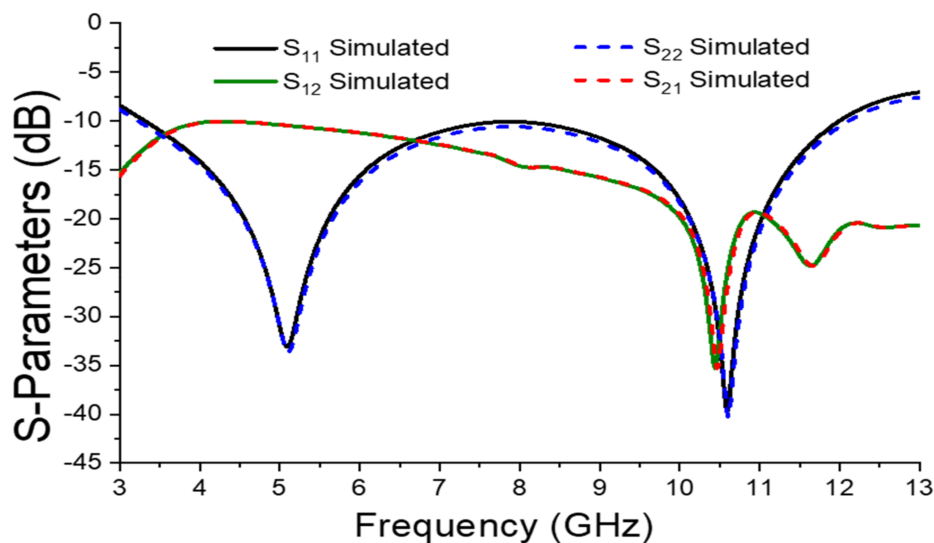
Figure 5 depicts the geometry of the proposed two-antenna MIMO without and with loading the decoupling structure. As seen from Figure 5a, two identical monopole antenna elements (ANT#3) are closely deployed side by side of each other, with a gap distance of only  $0.12\lambda$  ( $\lambda$  is the free space wavelength at 5 GHz), and it is much narrower than the one reported in [9], with a gap distance of  $>1/4\lambda$ . Nevertheless, this gap distance can still provide enough space for the deployment of a decoupling structure (5 concentric ring elements), as shown in Figure 5b. Furthermore, this narrow gap distance can also ensure that the desired antenna and MIMO diversity performances remain unaffected in a rich multipath fading environment.



**Figure 5.** Geometry of the proposed two-antenna MIMO, (a) without decoupling structure, (b) with decoupling structure.

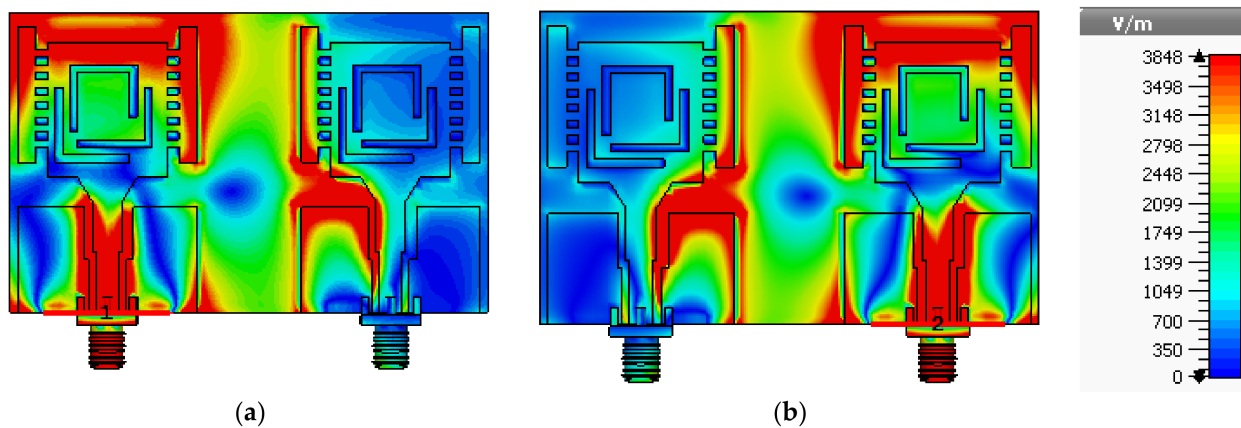
#### 4.1. Analysis of the Two-Antenna MIMO without Decoupling Structure

Figure 6 plots the simulated reflection coefficient ( $S_{11}$  and  $S_{22}$ ) and isolation ( $S_{12}$  and  $S_{21}$ ) curves of the proposed two-antenna MIMO without loading the decoupling structure. Here, both the  $S_{11}$  and  $S_{22}$  are almost identical, and they have shown wide 10-dB impedance bandwidths of 81.08% (3.3–7.8 GHz) and 40% (8.0–12.0 GHz). However, the isolation level ( $S_{12}$  or  $S_{21}$ ) between the two antenna elements at around 4 GHz is approximately 10 dB, which is undesirable because, as per the requirement of industry and IEEE standards, the minimum isolation between two adjacent antenna elements should be greater than 15 dB so that each antenna element will produce independent communication paths, resulting in a higher data rate as well as uninterrupted internet access, wireless and satellite services.



**Figure 6.** Simulated S-parameters of the proposed two-antenna MIMO without loading the decoupling structure.

Figure 7 shows the electric field intensity (V/m) distribution across the proposed two-antenna MIMO at a resonant frequency of 5GHz. As shown in Figure 7a, when antenna element#1 is excited (while antenna element#2 is terminated by a 50 Ω load impedance), one can see that the antenna element#2 is highly influenced (coupled) by the strong electric field generated from the antenna element#1. It is also validated when antenna element#2 is excited, while antenna element#1 is terminated with a 50 Ω load impedance, as seen in Figure 7b. This clearly indicates that the antenna elements are invincibly mutually coupled with each other.



**Figure 7.** Electric field intensity (V/m) of the proposed two-antenna MIMO without decoupling structure, (a) antenna element#1 excited at 5GHz, (b) antenna element#2 excited at 5GHz.

4.2. Analysis of the Proposed Two-Antenna MIMO with Decoupling Structure

To reduce the mutual coupling between the two antenna elements, a decoupling structure is loaded between the antenna elements (within the 0.12λ gap distance), as shown in Figure 5b, in which the decoupling structure is comprised of five concentric ring elements. In this case, each ring has an inner and outer radius of 1 mm and 1.5 mm, respectively, and they are printed vertically with a gap distance of 1 mm away from each other. Furthermore, a very thin strip of 0.25 mm in height is added in between the antenna elements in order to connect the ground planes. By further observing the reflection coefficient curves in Figure 8, it is apparent that the deployment of the decoupling structure, as well as connecting the ground plane, does not affect the impedance bandwidth (as seen from the S<sub>11</sub>/S<sub>22</sub> curves)

of both antenna elements. Notably, the decoupling structure has significantly enhanced the isolation level between the two antenna elements, and a level of  $>20$  dB (seen from  $S_{12}/S_{21}$  curves) is observed which was verified by applying two plane waves across the length of the decoupling structure [22]. The isolation of below  $-20$  dB is achieved as the equidistance spaced circles act as reflectors and absorb the surface wave which, therefore, serves as a wide stop band filter and nullifies the surface wave propagation between Ant. 1 and Ant. 2 [23].

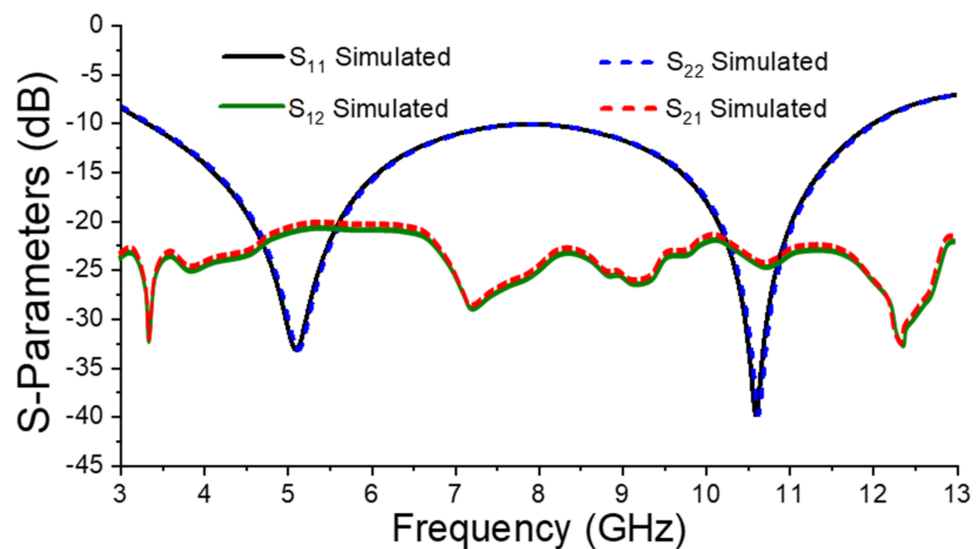


**Figure 8.** S-parameters of two-port MIMO Antenna with decoupling structure.

To further comprehend the validation of the isolating structure, electric field distribution (V/m) analysis at a resonant frequency of 5GHz is shown in Figure 9, where it can be easily seen that the antenna element#2 is being prevented from the strong electric field of antenna element#1, which is due to the five concentric ring elements that act as a band stop filter to attenuate the correlated signals coming out from antenna element#1. The same phenomenon is also shown when antenna element#2 is excited, while antenna element#1 is terminated with a  $50 \Omega$  load impedance.

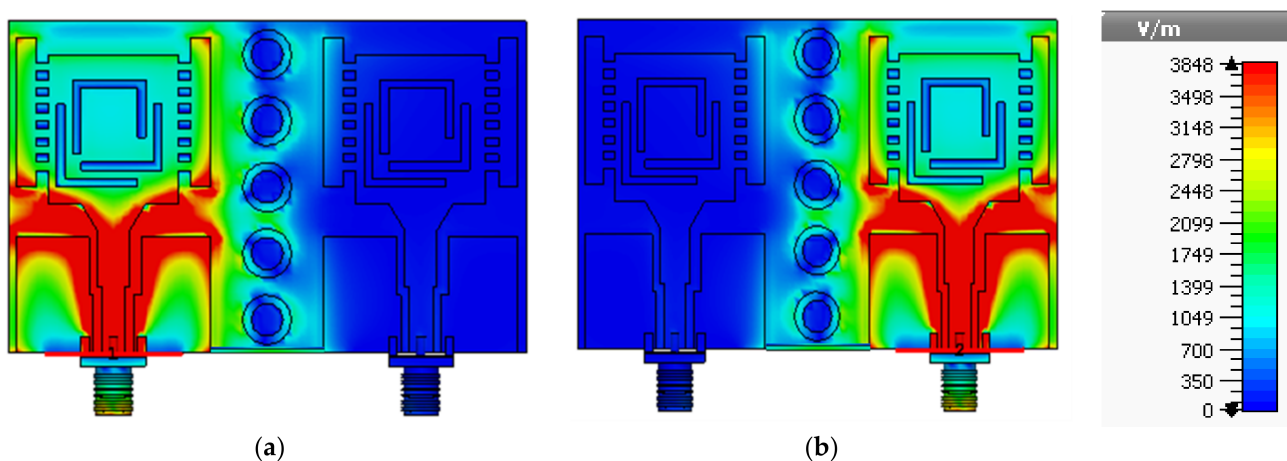


**Figure 9.** Electric field intensity (V/m) of the proposed two-antenna MIMO with decoupling structure, (a) antenna element#1 excited at 5GHz, (b) antenna element#2 excited at 5 GHz.

## 5. Results and Discussion of the Proposed Two-Antenna MIMO

To implement the proposed two-antenna MIMO for wireless and satellite applications functioning in Sub-6 GHz 5G NR, 802.11ac/ax, C-band, and X-band, a prototype is manu-

factured and depicted in Figure 10. The scattering, radiating and diversity performances of the fabricated proposed prototype are verified with simulated performances, and they are discussed in the below sub-sections. Notably, when analysing the performances of the two-antenna MIMO, only one antenna element is excited, whereas the other antenna element is terminated with a  $50 \Omega$  load impedance. The Rohde & Schwarz ZNH18 network analyser, having a frequency range of 30 kHz to 18 GHz, was used for measuring S-parameters, whereas the anechoic chamber was used to measure the radiation characteristic of the proposed antenna.

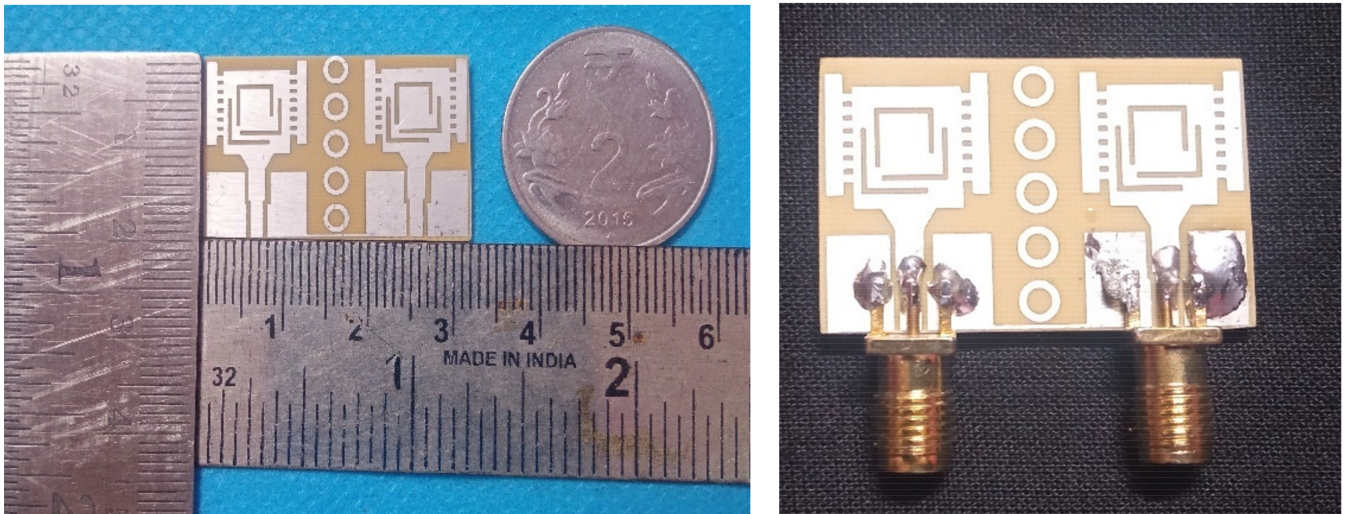


**Figure 10.** Fabricated prototype of the proposed two-antenna MIMO.

#### 5.1. Simulated and Measured Reflection Coefficient and Isolation

As the reflection coefficient ( $S_{11}$ ) and isolation ( $S_{12}$ ) are analogous to  $S_{22}$  and  $S_{21}$ , respectively, Figure 11 only shows the simulated and measured  $S_{11}$  and  $S_{12}$  characteristics of the proposed two-antenna MIMO. In this figure, both simulated and measured results are well-validated with each other, and the observed deviation (especially in the high band) may be due to manufacturing tolerances and minor fabricating errors. Nevertheless, a dualband operation is clearly shown in Figure 11a, in which the measured low band and high band operation have exhibited a wide 10-dB impedance bandwidth of 80.54% (3.3–7.75 GHz) and 41.2% (7.9–12.0 GHz), respectively, while isolation larger than 20 dB was achieved across the two operating bands of interest, as seen in Figure 11b.

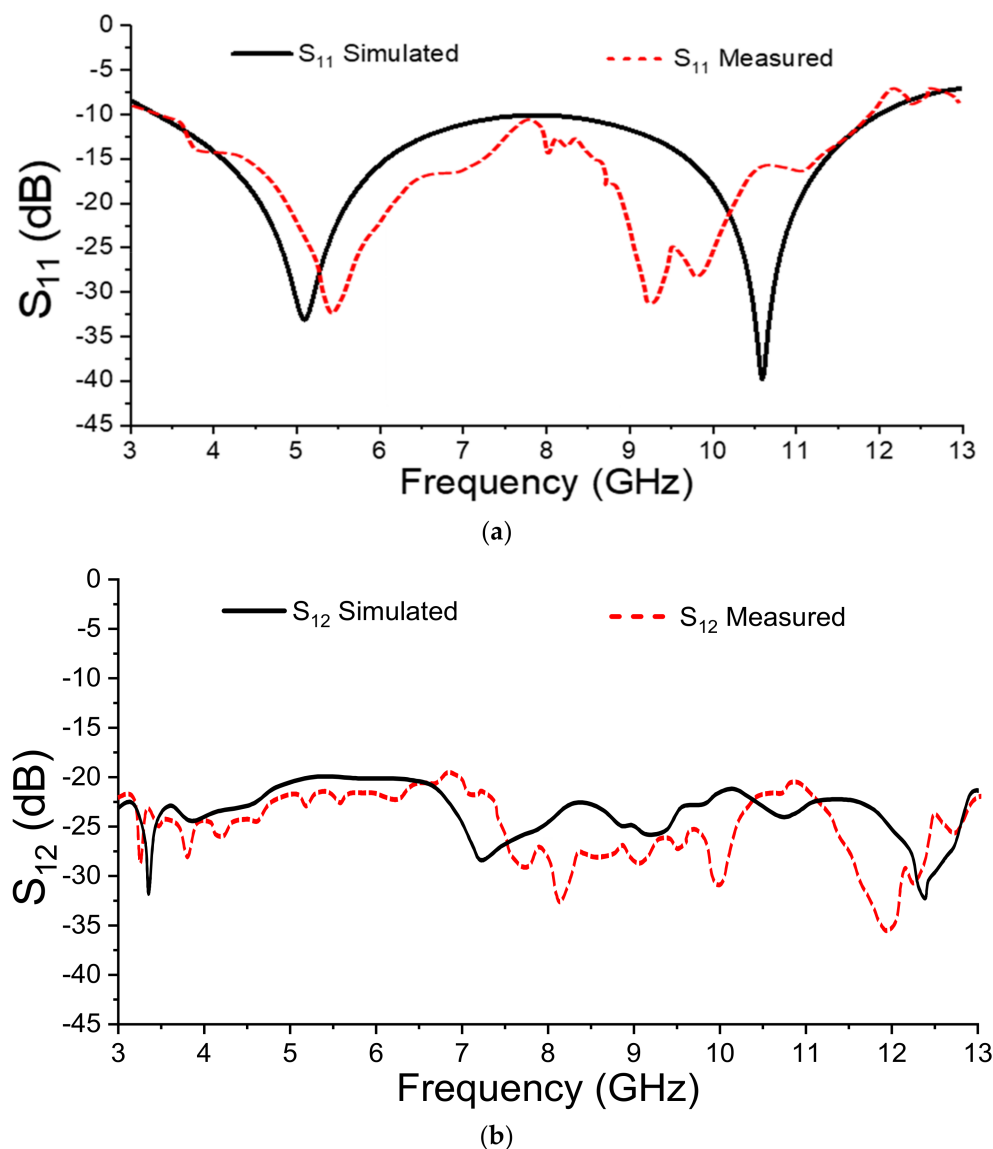


**Figure 11.** Simulated and measured S-parameters of the proposed two-antenna MIMO, (a) reflection coefficient,  $S_{11}$ , (b) isolation,  $S_{12}$ .

### 5.2. Simulated and Measured Far Field Radiation Patterns

The radiation patterns of the proposed two-antennas MIMO across the E-plane and H-plane are depicted in Figure 12a–d. As shown in Figure 12a,b, across the two bands of interest, 5.0 GHz and 10.5 GHz, the two antenna elements at the E-plane are exhibiting near-omnidirectional patterns and 8-shaped patterns for the co-polarisation (co-polar) and cross-polarisation (cross-pol) radiation, respectively. Furthermore, it is also noteworthy that at both frequencies, the radiation patterns of antenna element#1 are exactly mirror images of the ones shown in antenna element#2. As for its H-plane counterparts, as shown in Figure 12c,d, across the two bands of interest, 5.0 GHz and 10.5 GHz, respectively, the two antenna elements at the H-plane are exhibiting bi-directional patterns (co-polar) and broadside patterns (cross-pol). The above results demonstrated that the proposed two-antenna MIMO has offered acceptable radiation characteristics to meet the desire MIMO diversity performances.

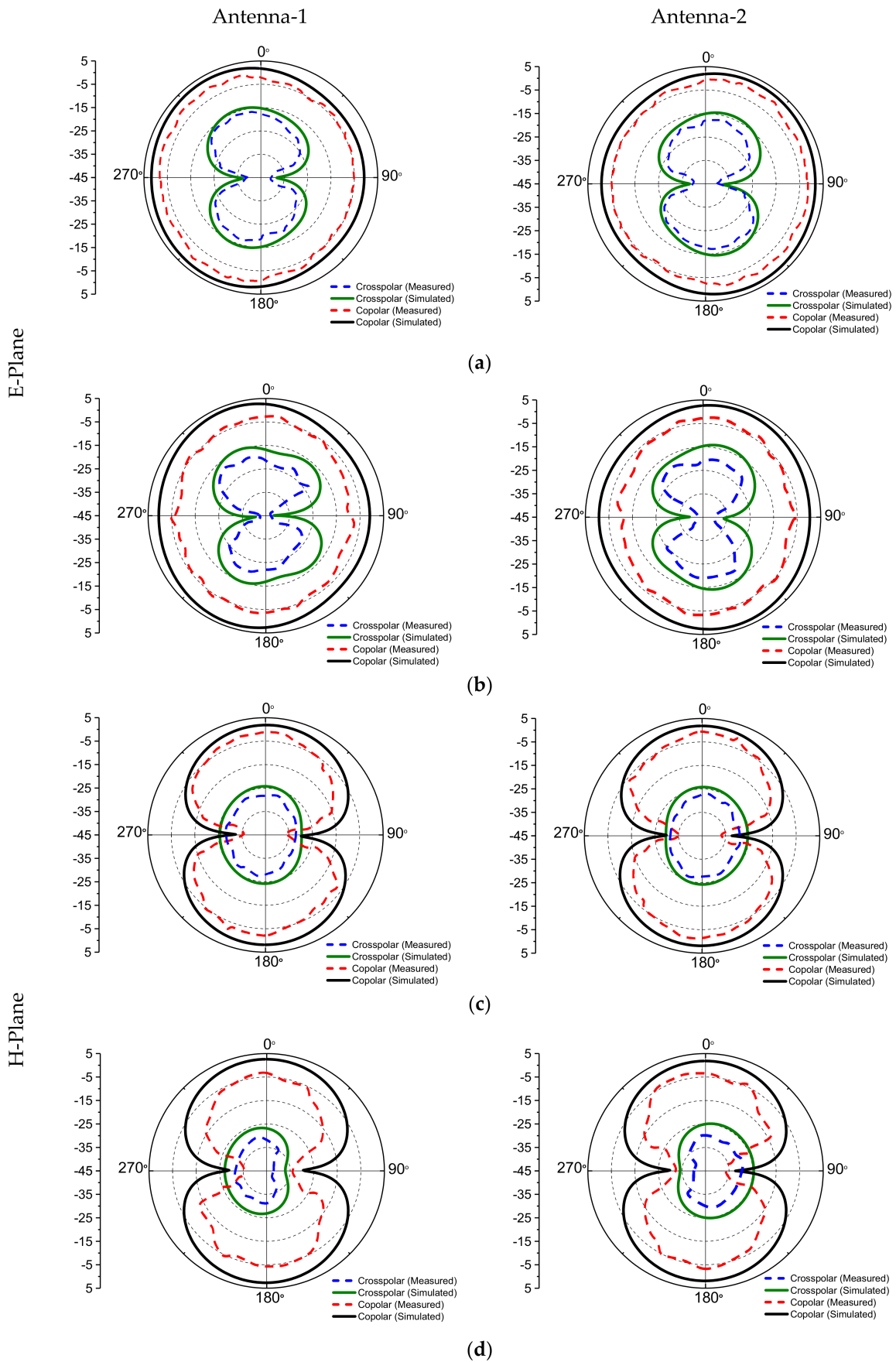


Figure 12. Radiation patterns of antenna element#1 and antenna element#2, (a) 5.0 GHz, E-plane, (b) 10.5 GHz, E-plane, (c) 5.0 GHz, H-plane, (d) 10.5 GHz, H-plane.

### 5.3. Simulated and Measured Realised Gain and Radiation Efficiency

As the two antenna elements are identical to each other, we only plot the gain and efficiency of antenna element#1, and they are illustrated in Figure 13. In this figure, between 3.5 GHz and 12 GHz, the simulated gain was 3.0–4.66 dBi, while the measured one was 2.65–4.00 dBi. As for its corresponding radiation efficiency, the simulated one was ranging from 72.5% to 82%, while the measured one was between 69.64% and 76.8%. Thus, the proposed two-antenna MIMO has exhibited stable gain and efficiency throughout the operating bands of interest. The simulated and measured peak gain and peak efficiency are compared and presented in Table 2, and one can see that these results can ensure good quality of communication.

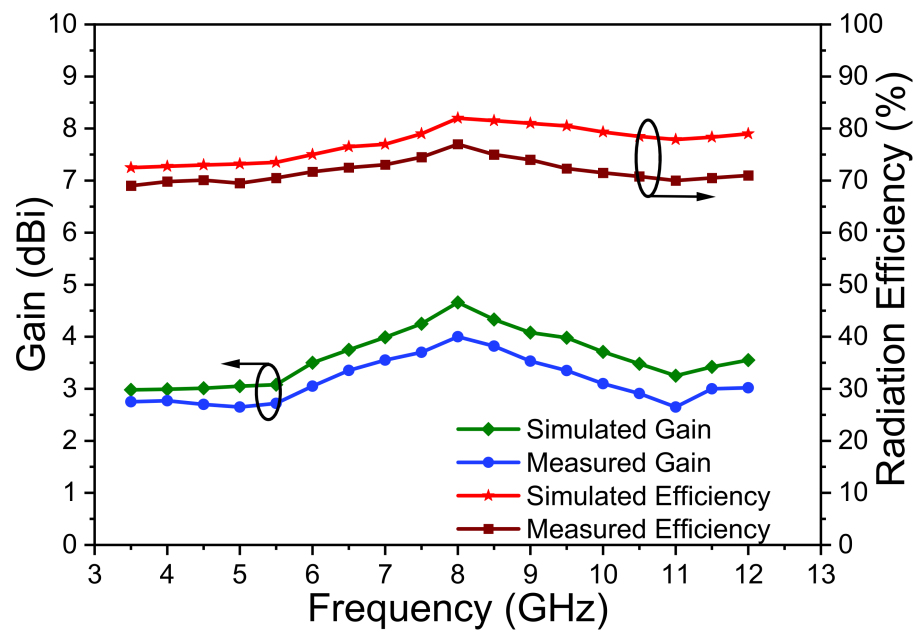


Figure 13. Gain and radiation efficiency of the proposed two-port MIMO Antenna.

Table 2. Comparison of Simulated and Measured Peak Gain and Peak Efficiency.

Functioning Band	Simulated Peak Gain (dBi)	Measured Peak Gain (dBi)	Simulated Peak Efficiency ( $\eta$ )%	Measured Peak Efficiency ( $\eta$ )%
Sub-6 GHz 5G NR & C-band uplink	3.00	2.77	72.99	70.10
IEEE 802.11ac	3.08	2.72	73.50	70.50
IEEE 802.11ax & C-band downlink	3.75	3.35	76.50	72.49
X-band	3.48	2.91	78.48	70.80

## 6. Diversity Performance Analysis

To prove the potency of the proposed two-antenna MIMO, the diversity performances matrix, such as ECC, DG, MEG, CCL, channel capacity, and TARC, are very essential, and thus they are further verified through simulation as well as measurement.

### 6.1. Envelope Correlation Coefficient (ECC)

To know how independently antenna elements radiate throughout the operating band, the ECC is a very essential parameter to be investigated. Ideally, the ECC value should be equal to zero, which indicates that the antenna elements radiate independently by producing uncorrelated radiations. However, in a rich fading environment, the value of ECC is not equivalent to zero. Notably, the ECC value of the proposed two-antenna MIMO

can be calculated via the S-parameters, as denoted in Equation (1); however, one condition to be noted is that the two antenna elements must have an efficiency of near 100%, so that much accurate ECC can be determined. Thus, it is always better to apply Equation (2) via the far-field radiation patterns to determine the ECC, as the calculation of ECC via this equation is more accurate.

$$\rho_e = \frac{|S_{11} * S_{12} + S_{21} * S_{22}|^2}{(1 - |S_{11}|^2 - |S_{21}|^2)(1 - |S_{22}|^2 - |S_{12}|^2)} \tag{1}$$

$$\rho_e = \frac{\left| \iint_{4\pi} [\vec{F}_1(\theta, \varphi) * \vec{F}_2(\theta, \varphi)] d\Omega \right|}{\iint_{4\pi} |\vec{F}_1(\theta, \varphi)|^2 d\Omega \iint_{4\pi} |\vec{F}_2(\theta, \varphi)|^2 d\Omega} \tag{2}$$

where  $\vec{F}_i(\theta, \varphi)$  is the three-dimensional field pattern of the antenna, when  $i$ th port is excited.  $\Omega$  is solid angle.

Figure 14 shows the ECC values for various frequency ranges. It is seen that the ECC values obtained from Equations (1) and (2) are well below 0.05, which are very close to zero throughout the bands of interest of the proposed two-antenna MIMO. This confirms that both the antenna elements are uncorrelated from each other, and hence contribute to increasing the data rate of the system.

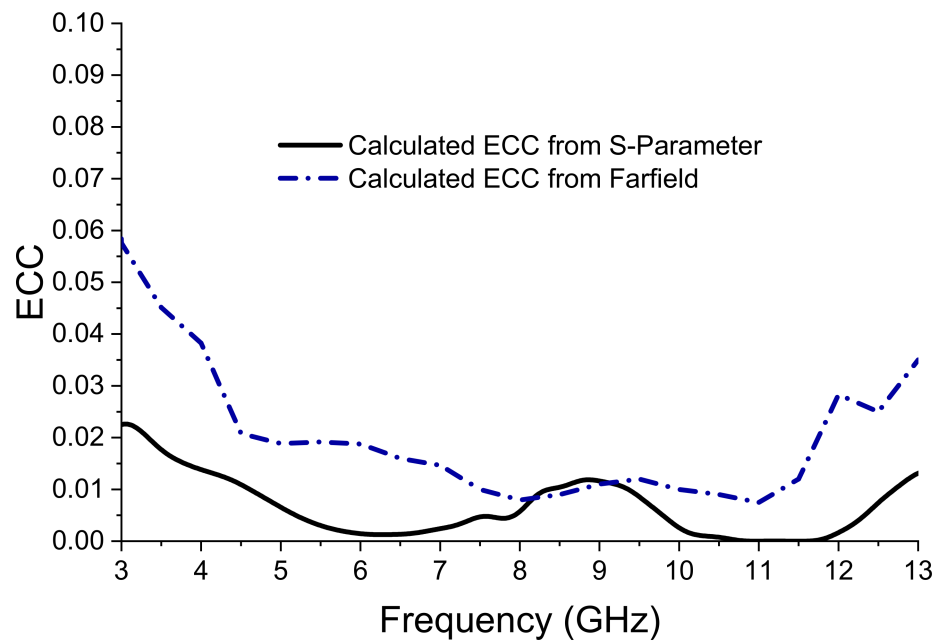


Figure 14. ECC of the proposed two-antenna MIMO.

6.2. Diversity Gain (DG) dB

The DG is another metric of interest as it helps the MIMO antenna to resolve multipath signals, thus improving the receiver’s ability to recover intelligent data from multipath signals at a fixed rate of transmission. The DG is the parameter used to determine the increment in signal to noise ratio (SNR) magnitude of each path due to the introduction of a spatial diversity scheme, and it is calculated by using the below formula mentioned in Equation (3).

$$DG = 10\sqrt{1 - |\rho_e|^2} \tag{3}$$

Figure 15 shows the DG of the proposed two-antenna MIMO. The calculated DG values obtained from the far-field and S-parameters are very close to 10 dB. This confirms

that both the antenna elements are strongly uncorrelated with each other and are good candidates for MIMO applications.

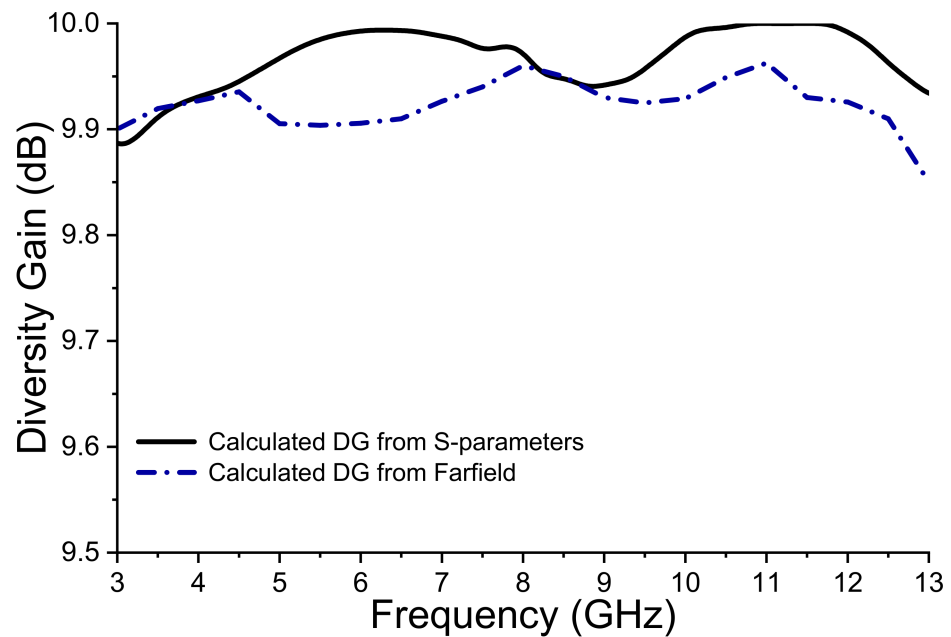


**Figure 15.** DG of the proposed two-antenna MIMO.

### 6.3. Mean Effective Gain (MEG)

The MEG determines the performance of antenna elements in a rich multipath fading practical environment. *MEG* is the ratio of mean received power to the mean incident power at the antenna element, and it is obtained using the efficiency method as denoted in Equation (4).

$$MEG_i = 0.5\mu_{irad} = 0.5 \left( 1 - \sum_{j=1}^K |S_{ij}|^2 \right) \quad (4)$$

where  $K$  is the number of antenna elements, ' $i$ ' is the excited antenna, and  $\eta_{irad}$  is the radiation efficiency of the  $i$ th antenna.

Further Solving Equation (4), the *MEG* of each antenna element can be computed by using Equations (5) and (6):

$$MEG_1 = 0.5 \left( 1 - |S_{11}|^2 - |S_{12}|^2 \right) \quad (5)$$

$$MEG_2 = 0.5 \left( 1 - |S_{21}|^2 - |S_{22}|^2 \right) \quad (6)$$

where,  $MEG_1$  and  $MEG_2$  are the *MEG* of antenna element#1 and antenna element#2, respectively. By observing Figure 16, one can see that the calculated *MEG* of the two antenna elements is identical (approximately  $-3$  dB) across the bands of interest, thus their corresponding ratio ( $MEG_1/MEG_2$ ) is one. Table 3 concludes the *MEG* values of the proposed two-antenna MIMO. In this table, the two antenna elements have acquired very good values, which ascertains that the proposed two-antenna MIMO has a maximum *DG*, better isolation across functioning bands, and smaller losses in diversity performances. Moreover, because the *MEG* ratios of the two antenna elements are closer to 1, it also validates better diversity performance from the proposed two-antenna MIMO under a very rich multipath fading environment of wireless channels.

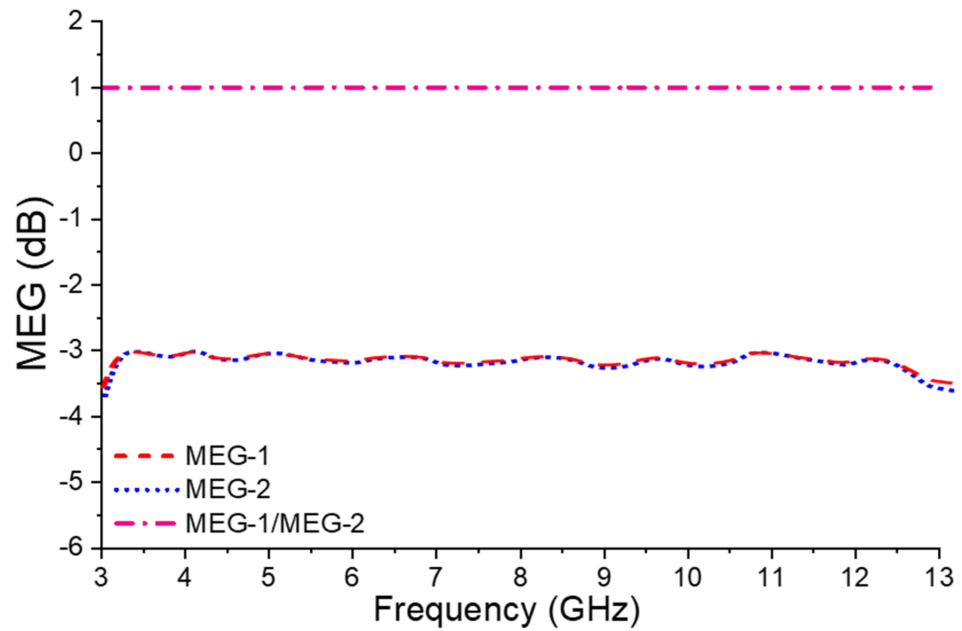


Figure 16. MEG of the proposed two-antenna MIMO.

Table 3. Mean effective gains (MEG) of the proposed two-antenna MIMO.

Frequency (GHz)	MEG (-dB) of Antenna Elements			
	Antenna Element#1	Antenna Element#2	Ratio of Antenna Element#1/Antenna Element#2	Ratio of Antenna Element#2/Antenna Element#1
Sub-6 GHz 5G and C-band uplink	-3.10	-3.11	0.99	1.00
IEEE 802.11ac	-3.21	-3.22	0.99	1.00
IEEE 802.11ax 5G and C-band downlink	-3.15	-3.14	1.00	0.99
X-band	-3.05	-3.04	1.00	0.99

6.4. Total Active Reflection Coefficient (TARC)

The TARC validates the diversity performance of a MIMO antenna and is calculated by using the below Equation (7).

$$\Gamma = \frac{\sqrt{(|S_{ii} + S_{ij}e^{j\theta}|^2) + (|S_{ji} + S_{jj}e^{j\theta}|^2)}}{\sqrt{2}} \tag{7}$$

where  $\theta$  is the input phase angle which is changed from  $0^\circ$  to  $180^\circ$  at an interval of  $30^\circ$ , and  $S_{ii}$  and  $S_{jj}$  are the reflection coefficients (dB) of antenna element#1 and antenna element#2, respectively.

Figure 17 illustrates the measured TARC values which are almost stable and below  $-10$  dB in the entire band. This validates that the proposed two-antenna MIMO has obtained good isolation, as well as serving as a good candidate for the integration with the phase shifter system.

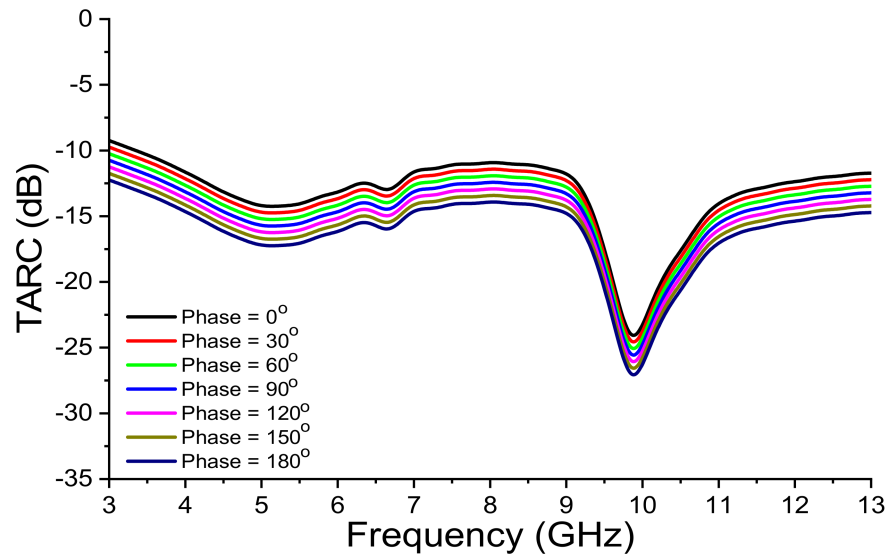


Figure 17. TARC of the proposed two-antenna MIMO.

6.5. Channel Capacity Loss (CCL)

The CCL is an essential metric to characterise the diversity performance of a MIMO antenna, as it confirms the higher bound on the rate of transmission. Thus, to ensure a high data rate, the CCL values must be below 0.5 bits/s/Hz across the operational band, and it is estimated by the following Equations (8) to (13).

$$C_{loss} = -\log_2 \det(\mu^R) \tag{8}$$

where,  $\Psi^R$  is the correlation matrix and is described as:

$$\mu^R = \begin{bmatrix} \mu_{11} & \mu_{12} \\ \mu_{21} & \mu_{22} \end{bmatrix} \tag{9}$$

where,

$$\mu_{11} = 1 - (|S_{11}|^2 + |S_{12}|^2) \tag{10}$$

$$\mu_{12} = -(S_{11} * S_{12} + S_{21} * S_{22}) \tag{11}$$

$$\mu_{21} = -(S_{22} * S_{21} + S_{12} * S_{11}) \tag{12}$$

$$\mu_{22} = 1 - (|S_{22}|^2 + |S_{21}|^2) \tag{13}$$

The simulated and measured CCL values of the proposed two-antenna MIMO using the S-parameters are demonstrated in Figure 18. Here, average values of CCL less than 0.35 bits/s/Hz are observed in the entire band, which ensure a better performance of the MIMO antenna by fulfilling the limits defined by the industry standards. Furthermore, the small discrepancy observed between the simulated and measured CCL values could be because of fabrication inaccuracies.

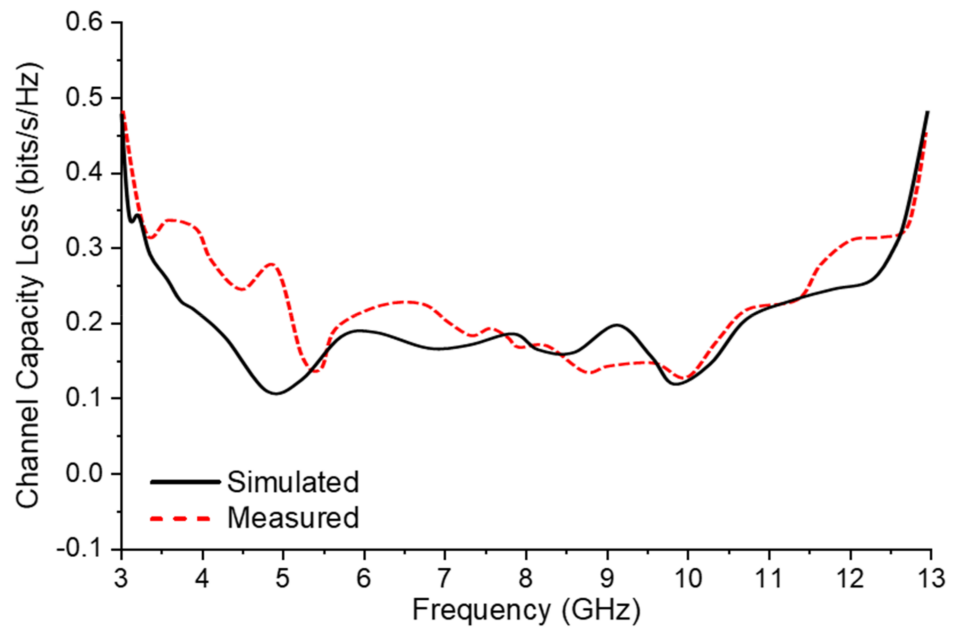


Figure 18. Channel Capacity Loss of the proposed two-antenna MIMO.

6.6. Channel Capacity (bits/s/Hz)

Channel capacity is a vital parameter used to calculate the multiplexing performance of the MIMO antenna, which is calculated using the equation in [20]. Figure 19 depicts the comparison graph of the channel capacity for the SISO and MIMO antenna. From Figure 19 it is easily observed that the channel capacity of the proposed two-antenna MIMO is greater than 10.00 bits/s/Hz in the entire band of interest, that is approximately 1.78 times higher as compared to the maximum limit of an ideal SISO antenna (approx. 5.65 bps/Hz). Further, it is also noticed that the channel capacity values are very near to the maximum limit for an ideal  $2 \times 2$  MIMO system (11.35 bps/Hz).

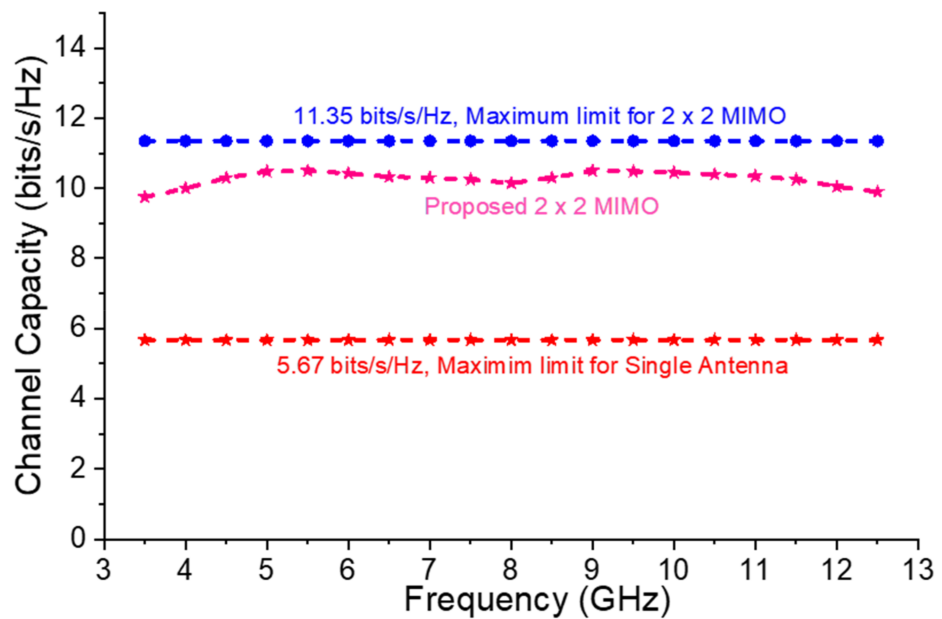


Figure 19. Channel Capacity of the proposed two-antenna MIMO.

## 7. Performance Comparison of the Proposed Two-Antenna MIMO with Existing State of Arts

The performance comparison of the proposed two-antenna MIMO with other existing two-antenna MIMO types, including bandwidth, dimensions, decoupling structure, gain, efficiency, ECC, and DG are mentioned in Table 4. Here, it is observed that the proposed two-antenna MIMO has exhibited wide dual impedance bandwidths with compact dimensions and good ECC and DG values.

**Table 4.** Performance comparison of proposed two-antenna MIMO with existing state of art.

Ref	Dimension (mm <sup>3</sup> )	Sub	BW (GHz)	Gain (dBi)	ECC	DG	Isol (dB)	Decoupling Structure
[1]	32 × 98 × 1	FR-4	0.6–0.7 1.7–1.9 2.4–2.7 3.2–4.1 5.1–5.9	5.14	0.04	9.8	>15	Not used
[2]	56 × 37 × 1.6	FR-4	2.24–2.50 3.60–3.99 4.40–4.60 5.71–5.90	2	0.08	9.5	>15	Not used
[4]	70 × 52 × 1.6	FR-4	3.10–3.21 6.20–6.33 7.60–7.90	5.84	0.025	9.5	>31	Not used
[9]	90 × 21 × 1.6	FR-4	2.22–2.54 3.14–3.90 5.30–5.90	3.22	0.01	10	>20	Not used
[10]	34 × 34 × 1.44	FR-4	3.50–3.60 5.00–5.40	4.7	0.01	-	>19	U-shape slot in ground plane
[13]	20 × 35 × 0.8	FR-4 epoxy	3.34–3.87	2.5	0.01	-	>20	T-shape ground stub
[15]	59 × 55 × 8.1	FR-4	3.00–7.00	4	0.2	8.94	>20	DGS
[18]	38.2 × 95.94 × 1.6	FR-4	2.43–2.50	4.25	0.008	9.99	>24	Fractal EBG
[19]	55 × 28 × 1.6	FR-4	2.01–3.92	2	0.01	9.8	>15	EBG
[20]	100 × 60 × 1	Jeans	1.34–3.92 4.34–6.34	5	0.04	9.0	>18	Meta-Inspired
[21]	47.5 × 40 × 1.6	FR-4	3.35–3.78	3.5	0.05	-	>15	Metamaterial
This Work	32 × 20 × 0.8	FR-4	3.3–7.8 8.0–12.0	4.0	0.05	9.9	>20	Concentric Rings

From the above table, the following features of the proposed two-antenna MIMO are observed:

1. It has the smallest physical dimensions (volume size) as compared to all the antennas mentioned in Table 1.
2. Unlike [10,13,16–19], the proposed one has exhibited a very wide dual bandwidth operation.
3. It has a higher gain, as compared to [2,9,10,13,15–17,19].
4. Unlike [2,15], the proposed one has higher ECC and DG.
5. The decoupling structure applied in this work is very simple and easy to design, and it can yield high isolation of >20 dB, as compared to antennas reported in [1,2,4,9].

## 8. Conclusions

A two-antenna MIMO functioning in the Sub-6 GHz 5G NR, IEEE 802.11ac/ax, C-band, and X-band has been successfully studied. Besides showing very wide dual 10-dB impedance bandwidths of 81.08% (3.3–7.8 GHz) and 40% (8.0–12.0 GHz), the proposed two-antenna MIMO has also exhibited a gain >3 dBi and efficiency greater than 69% throughout the two bands of interest. By loading a decoupling structure (five concentric ring elements) between the two adjacent antenna elements, a very desirable isolation above 20 dB is obtained. The MIMO performance metrics, such as ECC (<0.05), DG (>9.9 dB), CCL (<0.35/bits/s/Hz), TARC (<−10 dB), and MEG1/MEG2 ratio (approximately equal to 1) are investigated, and their corresponding values are well within the acceptable practical values. Furthermore, the calculated channel capacity is larger than 10.00 bits/s/Hz. Therefore, because of its compact size, good scattering and radiation characteristics, better diversity performance, the proposed two-antenna MIMO is a potential candidate in futuristic devices for above aforementioned wireless and satellite applications.

**Author Contributions:** Conceptualization, A.G.A., J.K. and C.-Y.-D.S.; methodology, A.D.; software, A.G.A. and J.K.; validation, J.K., C.-Y.-D.S. and A.P.; formal analysis, A.G.A. and A.D.; investigation, A.G.A. and J.K.; writing—original draft preparation, A.G.A., J.K. and A.D.; writing—review and editing, J.K. and A.D.; visualization, A.G.A.; supervision, C.-Y.-D.S. and A.P.; project administration, A.P. and J.K.; funding acquisition, A.G.A. All authors have read and agreed to the published version of the manuscript.

**Funding:** This research received no external funding.

**Data Availability Statement:** All data are included within manuscript.

**Conflicts of Interest:** The authors declare no conflict of interest.

## References

- Hassan, M.M.; Zahid, Z.; Khan, A.A.; Rashid, I.; Rauf, A.; Maqsood, M.; Bhatti, F.A. Two element MIMO antenna with frequency reconfigurable characteristics utilizing RF MEMS for 5G applications. *J. Electromagn. Waves Appl.* **2020**, *34*, 1210–1224. [[CrossRef](#)]
- Chouhan, S.; Panda, D.K.; Kushwah, V.S.; Singhal, S. Spider-shaped fractal MIMO antenna for WLAN/WiMAX/Wi-Fi/Bluetooth/C-band applications. *AEU Int. J. Electron. Commun.* **2019**, *110*, 1–8. [[CrossRef](#)]
- Soltani, S.; Lotfi, P.; Murch, R.D. A Dual-Band Multiport MIMO Slot Antenna for WLAN Applications. *IEEE Antennas Wirel. Propag. Lett.* **2016**, *16*, 529–532. [[CrossRef](#)]
- Babu, K.V.; Anuradha, B. Design and performance analysis of tri-band Wang shaped MIMO antenna. *Int. J. Inf. Technol.* **2020**, *12*, 559–566. [[CrossRef](#)]
- El Ouahabi, M.; Zakriti, A.; Essaaidi, M.; Dkiouak, A.; Hanae, E. A miniaturized dual-band MIMO antenna with low mutual coupling for wireless applications. *Prog. Electromagn. Res. C* **2019**, *93*, 93–101. [[CrossRef](#)]
- Kulkarni, J.; Sim, C.Y.D.; Deshpande, V. Low-profile, compact, two port MIMO antenna conforming Wi-Fi-5/Wi-Fi-6/V2X/DSRC/INSAT-C for wireless industrial applications. In Proceedings of the IEEE 17th India Council International Conference (INDICON), New Delhi, India, 10–13 December 2020; pp. 1–5.
- Dkiouak, A.; Zakriti, A.; El Ouahabi, M. Design of a compact dual-band MIMO antenna with high isolation for WLAN and X-band satellite by using orthogonal polarization. *J. Electromagn. Waves Appl.* **2019**, *34*, 1254–1267. [[CrossRef](#)]
- Kumar, M.; Nath, V. Design and development of triple-band compact ACS-fed MIMO antenna for 2.4/3.5/5 GHz WLAN/WiMAX applications. *Analog. Integr. Circ. Sig. Process* **2020**, *103*, 461–470. [[CrossRef](#)]
- Ekrami, H.; Jam, S. A compact triple-band dual-element MIMO antenna with high port-to-port isolation for wireless applications. *Int. J. Electron. Commun.* **2018**, *96*, 219–227. [[CrossRef](#)]
- Islam, S.N.; Das, S. Dual-band CPW fed MIMO antenna with polarization diversity and improved gain. *Int. J. RF Microw. Comput. Eng.* **2020**, *30*, e22128. [[CrossRef](#)]
- Tiwari, R.N.; Singh, P.; Kanaujia, B.K.; Kumar, S.; Gupta, S.K. A low-profile dual band MIMO antenna for LTE/ Blue-tooth/Wi-Fi/WLAN applications. *J. Electromagn. Waves Appl.* **2020**, *34*, 1239–1253. [[CrossRef](#)]
- Kulkarni, J.; Desai, A.; Sim, C. Two port CPW-fed MIMO antenna with wide bandwidth and high isolation for future wireless applications. *Int. J. RF Microw. Comput. Eng.* **2021**, *31*, e22700. [[CrossRef](#)]
- Saurabh, A.K.; Meshram, M.K. Compact sub-6 GHz 5G-multipleinput- multiple-output antenna system with enhanced isolation. *Int. J. RF Microw. Comput. Aided Eng.* **2020**, *30*, e22246. [[CrossRef](#)]
- Khan, A.A.; Jamaluddin, M.H.; Aqeel, S.; Nasir, J.; Kazim, J.U.R.; Owais, O. Dual-band MIMO dielectric resonator antenna for WiMAX/WLAN applications. *IET Microwaves, Antennas Propag.* **2017**, *11*, 113–120. [[CrossRef](#)]

15. Kumari, T.; Das, G.; Sharma, A.; Gangwar, R.K. Design approach for dual element hybrid MIMO antenna arrangement for wideband applications. *Int. J. RF Microw. Comput. Eng.* **2018**, *29*, e21486. [[CrossRef](#)]
16. Kumar, M.; Nath, V. Analysis of low mutual coupling compact multi-band microstrip patch antenna and its array using defected ground structure. *Eng. Sci. Technol. Int. J.* **2016**, *19*, 866–874. [[CrossRef](#)]
17. Pandhare, R.A.; Zade, P.L.; Abegaonkar, M.P. Miniaturized microstrip antenna array using defected ground structure with enhanced performance. *Eng. Sci. Technol. Int. J.* **2016**, *19*, 1360–1367. [[CrossRef](#)]
18. Sharma, K.; Pandey, G.P. Two port compact MIMO antenna for ISM band applications. *Prog. Electromagn. Res. C* **2020**, *100*, 173–185. [[CrossRef](#)]
19. Biswas, A.K.; Chakraborty, U. Reduced mutual coupling of compact MIMO antenna designed for WLAN and WiMAX applications. *Int. J. RF Microw. Comput. Eng.* **2018**, *29*, e21629. [[CrossRef](#)]
20. Roy, S.; Chakraborty, U. Mutual Coupling Reduction in a Multi-band MIMO Antenna Using Meta-Inspired Decoupling Network. *Wirel. Pers. Commun.* **2020**, *114*, 3231–3246. [[CrossRef](#)]
21. Wang, C.; Yang, X.; Wang, B. A metamaterial-based compact broadband planar monopole MIMO antenna with high isolation. *Microw. Opt. Technol. Lett.* **2020**, *62*, 2965–2970. [[CrossRef](#)]
22. Kulkarni, J.; Desai, A.; Sim, C.Y.D. Wideband four-port MIMO antenna array with high isolation for future wireless systems. *AEU-Int. J. Electron. Commun.* **2021**, *128*, 1–4. [[CrossRef](#)]
23. Pirasteh, A.; Roshani, S.; Roshani, S. Compact microstrip lowpass filter with ultrasharp response using a square-loaded modified T-shaped resonator. *Turk. J. Electr. Eng. Comput. Sci.* **2018**, *26*, 1736–1746. [[CrossRef](#)]